

Phase-sensitive evidence for $d_{x^2-y^2}$ -pairing symmetry in the parent-structure high- T_c cuprate superconductor $\text{Sr}_{1-x}\text{La}_x\text{CuO}_2$

Jochen Tomaschko,¹ Sebastian Scharinger,¹ Victor Leca,^{1,2} Joachim Nagel,¹ Matthias Kemmler,¹ Teresa Selistrowski,¹ Dieter Koelle,¹ and Reinhold Kleiner^{1,*}

¹*Physikalisches Institut–Experimentalphysik II and Center for Collective Quantum Phenomena in LISA⁺, Universität Tübingen, Auf der Morgenstelle 14, 72076 Tübingen, Germany*

²*National Institute for Research and Development in Microtechnologies, Molecular Nanotechnology Laboratory, Erou Iancu Nicolae Street 126A, RO-077190, Bucharest, Romania*

(Received 23 March 2012; published 7 September 2012)

We report on a phase sensitive study of the superconducting order parameter of the infinite layer cuprate $\text{Sr}_{1-x}\text{La}_x\text{CuO}_2$ (SLCO), with $x \approx 0.15$. For the study a SLCO thin film was grown epitaxially on a tetracrystal substrate and patterned into direct-current superconducting quantum interference devices (dc SQUIDs). The geometry was designed to be frustrated for $d_{x^2-y^2}$ -wave pairing, that is, the SQUID ring comprising the tetracrystal point contains one 0 Josephson junction and one π Josephson junction, if the order parameter has $d_{x^2-y^2}$ -wave symmetry. Our results show that SLCO indeed is a $d_{x^2-y^2}$ -wave superconductor. This symmetry thus seems to be inherent to cuprate superconductivity. Subdominant order parameter components can be ruled out at least on a 5% level and may not be a necessary ingredient of high- T_c superconductivity.

DOI: [10.1103/PhysRevB.86.094509](https://doi.org/10.1103/PhysRevB.86.094509)

PACS number(s): 74.72.Ek, 74.20.Rp, 74.50.+r, 85.25.Dq

I. INTRODUCTION

Since the discovery of high transition temperature (high- T_c) superconductivity in cuprates,¹ tremendous work has been performed on these materials. Researchers succeeded in increasing T_c from initially 30 to 135 K^{2–4} by synthesizing increasingly complex compounds. All these materials have in common that superconductivity resides in the copper oxide (CuO_2) planes where superconducting charge carriers, Cooper pairs, form. An “infinite layer” (IL) cuprate consisting essentially of CuO_2 planes is therefore of fundamental interest for all questions addressing the basics of high- T_c superconductivity, for example, in view of the still unknown pairing mechanism, which is one of the most important unsolved issues in condensed matter physics. In 1988, Siegrist *et al.* succeeded in synthesizing such a simple cuprate, which is also known as the “parent structure” of cuprate superconductors.⁵ Its CuO_2 planes are only separated by a single alkaline earth metal plane ($A = \text{Ca}, \text{Sr}$ or Ba), forming a $A\text{CuO}_2$ crystal. Upon electron doping, it turned out to be superconducting with maximum $T_c = 43$ K.^{6–9}

In contrast to conventional superconductors the high- T_c cuprates are low-dimensional doped Mott insulators with strongly correlated electrons or holes as charge carriers. The cuprates exhibit many unusual and often not well understood properties both in their normal state and superconducting state, like the appearance of a pseudogap or the (unconventional) symmetry of the superconducting order parameter.^{10–12} Due to their exceptionally simple structure, IL compounds could play a decisive role in resolving some of these issues, thus contributing to the general physics of strongly correlated electron systems. In the following we focus on the symmetry of the superconducting order parameter. For hole-doped cuprates $d_{x^2-y^2}$ -wave pairing is established.^{13–15} Also, the electron-doped T' compounds¹⁶ $L_{2-x}\text{Ce}_x\text{CuO}_4$ ($L = \text{La}, \text{Pr}, \text{Nd}, \text{Eu},$ or Sm) have been shown to be predominant $d_{x^2-y^2}$ -wave superconductors by a number of phase-sensitive experiments.^{17–20} Strikingly, for the parent compounds the pairing symmetry is

essentially still unknown since a variety of experimental tests yielded conflicting results.^{16,21–30}

Phase-sensitive tests, such as experiments on corner junctions,³¹ tricrystal rings,³² or tetracrystal SQUIDs,^{18,33,34} are widely recognized to provide clear evidence for the pairing symmetry of the order parameter.¹⁵ Such experiments rely on Josephson junctions, which for IL cuprate thin films became available only very recently.³⁵ Here we report on phase sensitive experiments on the IL compound $\text{Sr}_{1-x}\text{La}_x\text{CuO}_2$ (SLCO), using tetracrystal dc SQUIDs. Our data unambiguously show that SLCO has $d_{x^2-y^2}$ -wave symmetry which thus seems to be universal for the cuprate superconductors.

II. SAMPLE DESIGN AND FABRICATION

The SLCO dc SQUIDs were patterned on BaTiO_3 -buffered tetracrystal SrTiO_3 substrates. The geometry involved is designed to be frustrated for $d_{x^2-y^2}$ -wave pairing, that is, the SQUID ring comprising the tetracrystal point contains one 0 junction and one π junction, if the order parameter has $d_{x^2-y^2}$ -wave symmetry. This device will be referred to as π -design SQUID. Its geometry, together with the design of a reference SQUID, is sketched in Fig. 1. There are four grain boundaries (GBs), labeled 1–4. GBs 1–3 have misorientation angles of 30° , while the misorientation angle of GB 4 is 0° . The π -design SQUID comprises all GBs. GB 4 will not form a grain boundary junction (GBJ) due to its 0° misalignment angle, in contrast to GBs 1–3. GBs 2 and 3, having a width of $58 \mu\text{m}$, form the active Josephson junctions in the current and voltage lead configuration indicated in Fig. 1. The bias current also passes GBJ 1 which, however, is much longer (~ 1.5 mm) than GBJs 2 and 3 and thus will have a much higher critical current. Below we will see however that flux quanta (Josephson fluxons) can enter this GBJ, which thus cannot be ignored in the data analysis.

If SLCO were a $d_{x^2-y^2}$ -wave superconductor, one of GBJs 2 and 3 faces a sign change of the order parameter (GBJ

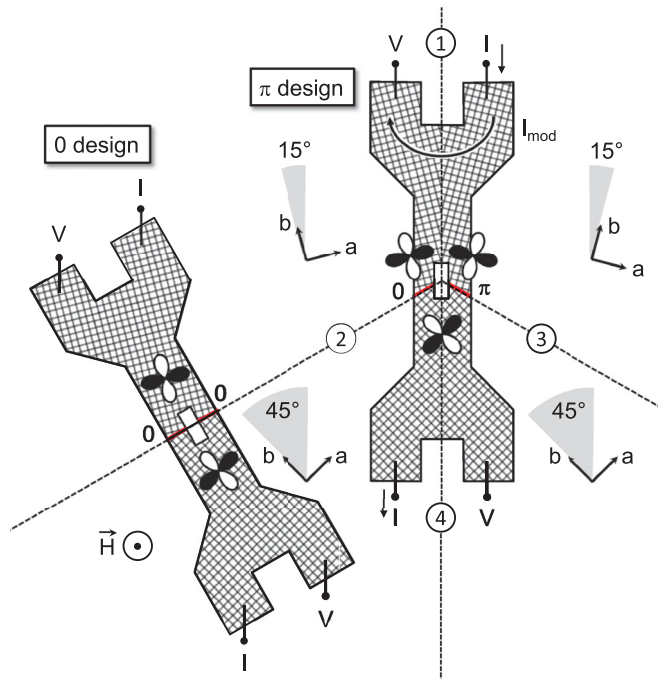


FIG. 1. (Color online) Schematic layout of the SQUIDs. The 0-design SQUID comprises two conventional GBJs (0 junctions) straddling a single 30° [001]-tilt grain boundary. The π -design SQUID comprises four GBJs. The misorientation angle of GB 4 is 0° . All other misorientation angles are 30° . The $d_{x^2-y^2}$ -wave order parameter is indicated by the cloverleaf structure consisting of white and black lobes, indicating the sign change of the order parameter. Leads for bias current I and voltage V are indicated. In some experiments, for the π -design SQUID we have also sent a current I_{mod} across GB 1. Magnetic fields have been applied perpendicular to the substrate plane.

3 in Fig. 1), thus forming a π Josephson junction. The other GBJs are conventional. The area of GBJs 2 and 3 is not much smaller than the area of the SQUID hole. In this “spatially distributed junction” design³⁶ the junction’s I_c vs H modulation (Fraunhofer pattern) is superposed on the SQUID modulation on a similar field scale. The (a)symmetry of the SQUID modulation relative to the Fraunhofer envelope allows us to detect residual fields and often also trapped magnetic flux.

The reference SQUIDs—there were two reference SQUIDs, producing very similar results—cross only one of the 30° GBs and incorporate two $50\ \mu\text{m}$ wide GBJs, which act as conventional junctions both for s -wave and $d_{x^2-y^2}$ -wave order parameters. Below, these devices will be referred to as the 0-design SQUIDs. Both the π -design SQUID and the reference SQUIDs had rectangular SQUID holes with an area $A_S = 50 \times 75\ \mu\text{m}^2$.

The samples have been fabricated by pulsed laser deposition, as described elsewhere.^{35,37,38} In brief, we first deposited a 25-nm-thick BaTiO_3 thin film on the SrTiO_3 tetracystal, acting as a buffer layer. This layer was followed by a 22-nm-thick SLCO thin film, with doping $x \approx 0.15$. Finally, a 10-nm-thick gold layer was evaporated *in situ*, protecting SLCO from degradation and acting as a resistive shunt for the GBJs. The SQUIDs were patterned by standard photolithography and argon ion

milling. The SLCO film had a critical temperature $T_c \approx 18\ \text{K}$. Electric transport measurements were performed at $T = 4.2\ \text{K}$ in a four-point configuration, with the sample mounted inside a noise-filtered, magnetically and radio frequency shielded probe in a liquid-helium Dewar. A SQUID amplifier was used to allow for low-noise measurements.

III. DETERMINATION OF JUNCTION AND SQUID PARAMETERS

Below we discuss data of one of the 0-design SQUIDs and of the π -design SQUID. The current voltage (IV) characteristics of these devices were nonhysteretic and could be well reproduced by the SQUID Langevin equations, extended by taking the nonzero junction width into account. Details can be found in Ref. 39, giving reasonable values for the junction parameters I_0 (maximum amplitude of Josephson current), R (junction resistance), and C (junction capacitance). The junctions of each device were symmetric in terms of I_0 , R , and C , with values $I_0 = 8.2\ \mu\text{A}$, $R = 0.92\ \Omega$, $C = 24\ \text{pF}$ (0-design SQUID) and $I_0 = 12.2\ \mu\text{A}$, $R = 0.87\ \Omega$, $C = 25\ \text{pF}$ (π -design SQUID). For the inductance parameter $\beta_L = 2I_0L/\Phi_0$, where Φ_0 is the magnetic flux quantum and L is the total inductance of the SQUID, we found $\beta_L = 1.4$ (0-design SQUID; $L = 177\ \text{pH}$) and 2.2 (π -design SQUID; $L = 187\ \text{pH}$), with an asymmetry $a_L = 0.05$ between the left and right arm of the SQUID (both designs). A fraction $f_J = 0.128$ (0-design SQUID) and $f_J = 0.12$ (π -design SQUID) of the flux Φ applied to the SQUID loop was coupled to each junction. The numbers for f_J were derived from an analysis of the SQUID critical current I_c vs applied field H (see below).

IV. CRITICAL CURRENT VS APPLIED MAGNETIC FIELD

Figure 2(a) shows the measured I_c vs H for the 0-design SQUID (black line). I_c was determined using a voltage

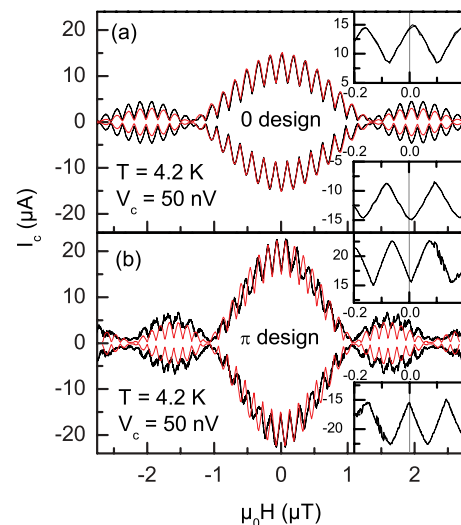


FIG. 2. (Color online) Critical current I_c vs applied magnetic field H of (a) the 0-design SQUID and (b) the π -design SQUID (black lines) together with calculated curves (red lines) for (a) a 0 SQUID and (b) a π SQUID. Insets show I_c vs H on expanded scales. A $50\ \text{nV}$ voltage criterion was used to determine I_c .

criterion $V_c = 50$ nV. To identify magnetic hysteresis effects, I_c vs H was traced from 2.8 to -2.8 μT and back to 2.8 μT . One observes a SQUID modulation with period $\mu_0\Delta H = 0.175$ μT on top of a Fraunhofer-like modulation, which is due to the finite junction size. No hysteresis is visible. The modulation period corresponds to an effective SQUID area of 1.18×10^4 μm^2 , pointing to a flux compression of about 3.15. This is reasonable for our structures.^{18,40} The insets of Fig. 2(a) show I_c vs H near $H = 0$ for both positive and negative I_c . The I_c maximum is close to $H = 0$, with a small offset of 10.6 nT for positive I_c and 5.2 nT for negative I_c . We attribute the asymmetry of ± 2.7 nT in offsets to an inductance asymmetry ($a_L = 0.05$) of the two SQUID arms and the average part of 7.9 nT to residual fields in the cryostat. The red line in Fig. 2(a) is a numerical calculation. It produces data very well inside the main maximum of the Fraunhofer envelope. The first Fraunhofer side maximum is lower in amplitude than the experimental data, presumably due to a field distribution inside the junction, which is more complex than the homogeneous flux density assumed in our model. Most importantly, however, we see that the 0-design SQUID behaves as it should be expected from a conventional 0-SQUID.

The measured I_c vs H of the π -design SQUID is shown by the black line in Fig. 2(b). Also here we have varied H from 2.8 to -2.8 μT and back to 2.8 μT . I_c is at a *minimum* near $H = 0$ —a feature which appears when one of the two Josephson junctions exhibits an additional π shift in its phase. At negative I_c the minimum is at $\mu_0 H \approx 0.15$ nT, while at positive I_c it appears at $\mu_0 H \approx 7.8$ nT, pointing to an offset field of about 4 nT and a small asymmetry in inductance ($a_L = 0.05$). The SQUID modulation period is $\mu_0\Delta H = 0.136$ μT , corresponding to an effective area of 1.52×10^4 μm^2 and a flux compression factor of 4.05. The overall modulation of I_c vs H is described reasonably well by numerical calculations (red line), however less well than I_c vs H of the 0-design SQUID.

A prominent feature are the jumps in I_c , visible at $\mu_0 H > 89$ nT at positive I_c and at $\mu_0 H < -80$ nT at negative I_c . There is only a very tiny hysteresis associated with these jumps, which is not even visible in Fig. 2(b). By comparing measured and calculated I_c vs H curves within the main Fraunhofer lobe one sees that the calculated curve exhibits one additional SQUID period. These features indicate that magnetic flux quanta enter the device at each jump. This effect was not visible for the 0-design SQUID. A strong candidate for flux entry is thus GBJ 1 which is absent in the reference SQUID. Note that the I_c jumps visible in Fig. 2(b) occur point symmetric, that is, at positive I_c they occur at positive fields, while at negative I_c the field is negative, with about the same amplitude as for positive I_c . This feature can also clearly be seen in V vs Φ patterns taken at many values of bias current (see Ref. 39). There we also show that the point symmetry in I_c vs H holds even for large values of H , and that applying an additional current I_{mod} across GBJ 1 alters the values of H in a way that is compatible with the notion of Josephson fluxons having entered GBJ 1.

V. SPATIALLY RESOLVED ANALYSIS OF TRAPPED FLUX

For a final proof we have imaged the current distribution of the π -design SQUID using low temperature scanning electron

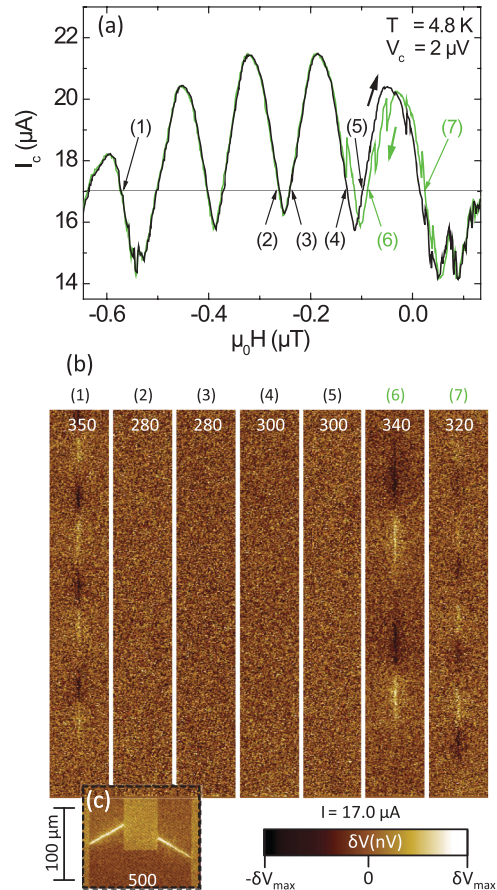


FIG. 3. (Color online) LTSEM data: (a) I_c vs H , as measured in the LTSEM setup (black and green lines distinguish sweep directions), (b) δV images, taken along GBJ 1 at $I = 17$ μA [horizontal line in (a)] at the magnetic field values (1)–(7) indicated in (a). Graph (c) shows a δV image of the SQUID hole and GBJs 2 and 3 at $I = 22$ μA and $\mu_0 H = -0.19$ μT . This image has been superposed to scale to image (b)-(2) in order to indicate the position of the SQUID hole. For each image δV_{max} is indicated inside the graphs.

microscopy (LTSEM). Details of the method can be found in Refs. 20 and 41. In brief, the pulsed electron beam, which is scanned across the sample, causes local heating by ~ 1 K. The measured integral quantity is the voltage V across the SQUID, which is biased slightly above I_c . The electron beam causes a change $\delta V(x, y)$ depending on the beam position (x, y) . When the beam is scanned across GBJs 2 and 3 near a I_c maximum, a positive signal appears, because I_c is lowered, causing a slight increase of V [cf. Fig. 3(c)]. When GBJ 1 is free of vortices no signal is expected from this GB. By contrast, when Josephson fluxons are present, local heating will alter the screening currents around the fluxons. In a heated area the Cooper pair density and thus the maximum supercurrent density is suppressed, causing an increase of the Josephson length λ_J and, thus, the fluxon is virtually deformed towards the heated area. When the electron beam is between the fluxon center and the SQUID hole this causes an increase of the fluxon's stray flux coupled to the SQUID and thus a change in I_c . In the opposite case the stray flux is decreased. A fluxon will thus appear as a bipolar signal $\delta V(x, y)$, with increased/decreased

voltage relative to the unperturbed value of V . In a similar way, Abrikosov vortices trapped in a $\text{YBa}_2\text{Cu}_3\text{O}_7$ SQUID,⁴¹ as well as Josephson fluxons having entered a GBJ,⁴² have been imaged by LTSEM.

Figure 3(a) shows I_c vs H , as measured in the LTSEM setup at $T = 4.8$ K using a voltage criterion $V_c = 2 \mu\text{V}$. There is a stronger offset field ($\sim 0.25 \mu\text{T}$) than in the transport setup, causing a shift by about 2 SQUID modulation periods. Due to the Fraunhofer envelope this shift is straightforward to recognize. The two sweep directions of H have been distinguished by black and green lines. There is a nonhysteretic region around the offset field; at larger values of H , I_c jumps occur, leading to magnetic hysteresis. δV images of GBJ 1 [cf. Fig. 3(b)] have been taken at $I = 17 \mu\text{A}$ at the field values indicated by labels (1)–(7) in Fig. 3(a). No contrast appears when the sample is biased near the offset field [images (2) and (3)] or at a field smoothly extending this I_c vs H pattern [images (4) and (5)]. By contrast, when I_c jumps have occurred, we observed a periodically modulated signal, having a period decreasing with the field amplitude H relative to the offset field [images (1), (6), and (7)]. This is very indicative of Josephson fluxons having entered GBJ 1. In Fig. 3(c) we also show a δV image of the area around the SQUID hole and GBJs 2 and 3. The image has been taken in a separate run because we did not want to disturb the images of Fig. 3(b) by scanning across these GBJs. It has been taken at the maximum of the SQUID modulation at $I = 22 \mu\text{A}$ and $\mu_0 H = -0.19 \mu\text{T}$. The image is superposed to scale to image Fig. 3(b)-(2), to give an impression of the position of the SQUID hole and GBJs 2 and 3 relative to the images of Fig. 3(b).

The LTSEM data clearly show that the I_c vs H region of interest is free of trapped flux; we thus feel safe in interpreting the π -design data in favor of a $d_{x^2-y^2}$ -wave symmetry of $\text{Sr}_{1-x}\text{La}_x\text{CuO}_2$.

VI. DISCUSSION OF SUBDOMINANT ORDER PARAMETERS

One may in addition ask about subdominant order parameters. A real superposition $d_{x^2-y^2} \pm s$ is not very likely due to the tetragonal crystal symmetry but, if present, could lead to

an asymmetry of the critical currents of GBJs 2 and 3 and, in consequence, to a similar shift as the one we interpreted in terms of an inductance asymmetry. On the other hand, the 0-design SQUID should not show this asymmetry and we thus believe that an inductance asymmetry is more likely. By contrast, a complex admixture of a subdominant order parameter would lead to a ground state phase different from π or 0. Then, the SQUID modulation would shift relatively to the Fraunhofer envelope, making the amplitude of the inner I_c maxima asymmetric. This effect is not observed at least on a $\sim 5\%$ level.

VII. CONCLUSIONS

In summary, our data clearly show that the superconducting order parameter of the infinite-layer high- T_c cuprate $\text{Sr}_{1-x}\text{La}_x\text{CuO}_2$ has $d_{x^2-y^2}$ -wave symmetry. The phase sensitive configuration used was a π SQUID patterned on a tetracystal. The parasitic effect of Josephson fluxons entering one of the grain boundary junctions has been ruled out by direct imaging of the local supercurrent distribution. $\text{Sr}_{1-x}\text{La}_x\text{CuO}_2$ has the most simple crystal structure of all high- T_c cuprates. We conclude that the $d_{x^2-y^2}$ -wave symmetry is inherent to cuprate superconductivity and neither restricted to hole doping nor related to the complex crystal structures that complicates an analysis of almost all other cuprate superconductors. Such a universal behavior is, for example, expected if Cooper pairing is mediated by antiferromagnetic spin fluctuations^{13,43} or in the recently proposed fluctuating Cu-O-Cu bond model.^{44,45} Subdominant order parameters are absent at least on a 5% level and may not be a necessary ingredient of high- T_c superconductivity.

ACKNOWLEDGMENTS

J.T. gratefully acknowledges support by the Evangelisches Studienwerk e.V. Villigst and J.N. by the Carl-Zeiss Stiftung. V.L. acknowledges partial financial support by a grant of the Romanian National Authority for Scientific Research, CNCS UEFISCDI, project number PN-II-ID-PCE-2011-3-1065. This work was funded by the Deutsche Forschungsgemeinschaft (project KL 930/11).

*kleiner@uni-tuebingen.de

¹J. G. Bednorz and K. A. Müller, *Z. Phys. B* **64**, 189 (1986).

²M.-S. Kim, M.-K. Bae, W. C. Lee, and S.-I. Lee, *Phys. Rev. B* **51**, 3261 (1995).

³Y. C. Kim, J. R. Thompson, J. G. Ossandon, D. K. Christen, and M. Paranthaman, *Phys. Rev. B* **51**, 11767 (1995).

⁴R. Puźniak, R. Usami, K. Isawa, and H. Yamauchi, *Phys. Rev. B* **52**, 3756 (1995).

⁵T. Siegrist, S. M. Zahurak, D. W. Murphy, and R. S. Roth, *Nature (London)* **334**, 231 (1988).

⁶M. G. Smith, A. Manthiram, J. Zhou, J. B. Goodenough, and J. T. Markert, *Nature (London)* **351**, 549 (1991).

⁷G. Er, S. Kikkawa, F. Kanamaru, Y. Miyamoto, S. Tanaka, M. Sera, M. Sato, Z. Hiroi, M. Takano, and Y. Bando, *Physica C* **196**, 271 (1992).

⁸J. D. Jorgensen, P. G. Radaelli, D. G. Hinks, J. L. Wagner, S. Kikkawa, G. Er, and F. Kanamaru, *Phys. Rev. B* **47**, 14654 (1993).

⁹N. Ikeda, Z. Hiroi, M. Azuma, M. Takano, Y. Bando, and Y. Takeda, *Physica C* **210**, 367 (1993).

¹⁰M. R. Norman and C. Pépin, *Rep. Prog. Phys.* **66**, 1547 (2003).

¹¹D. A. Bonn, *Nat. Phys.* **2**, 159 (2006).

¹²P. A. Lee, *Rep. Prog. Phys.* **71**, 012501 (2008).

¹³D. J. Scalapino, *Phys. Rep.* **250**, 329 (1995).

¹⁴D. J. V. Harlingen, *Rev. Mod. Phys.* **67**, 515 (1995).

- ¹⁵C. C. Tsuei and J. R. Kirtley, *Rev. Mod. Phys.* **72**, 969 (2000).
- ¹⁶N. P. Armitage, P. Fournier, and R. L. Greene, *Rev. Mod. Phys.* **82**, 2421 (2010).
- ¹⁷C. C. Tsuei and J. R. Kirtley, *Phys. Rev. Lett.* **85**, 182 (2000).
- ¹⁸B. Chesca, K. Ehrhardt, M. Möhle, R. Straub, D. Koelle, R. Kleiner, and A. Tsukada, *Phys. Rev. Lett.* **90**, 057004 (2003).
- ¹⁹Ariando, D. Darminto, H.-J. H. Smilde, V. Leca, D. H. A. Blank, H. Rogalla, and H. Hilgenkamp, *Phys. Rev. Lett.* **94**, 167001 (2005).
- ²⁰C. Gürlich, E. Goldobin, R. Straub, D. Doenitz, Ariando, H.-J. H. Smilde, H. Hilgenkamp, R. Kleiner, and D. Koelle, *Phys. Rev. Lett.* **103**, 067011 (2009).
- ²¹T. Imai, C. P. Slichter, J. L. Cobb, and J. T. Markert, *J. Phys. Chem. Solids* **56**, 1921 (1995).
- ²²C.-T. Chen, P. Seneor, N.-C. Yeh, R. P. Vasquez, L. D. Bell, C. U. Jung, J. Y. Kim, M.-S. Park, H.-J. Kim, and S.-I. Lee, *Phys. Rev. Lett.* **88**, 227002 (2002).
- ²³G. V. M. Williams, R. Dupree, A. Howes, S. Krämer, H. J. Trodahl, C. U. Jung, M.-S. Park, and S.-I. Lee, *Phys. Rev. B* **65**, 224520 (2002).
- ²⁴V. S. Zapf, N.-C. Yeh, A. D. Beyer, C. R. Hughes, C. H. Mielke, N. Harrison, M. S. Park, K. H. Kim, and S.-I. Lee, *Phys. Rev. B* **71**, 134526 (2005).
- ²⁵Z. Y. Liu, H. H. Wen, L. Shan, H. P. Yang, X. F. Lu, H. Gao, M.-S. Park, C. U. Jung, and S.-I. Lee, *Europhys. Lett.* **69**, 263 (2005).
- ²⁶K. H. Satoh, S. Takeshita, A. Koda, R. Kadono, K. Ishida, S. Pyon, T. Sasagawa, and H. Takagi, *Phys. Rev. B* **77**, 224503 (2008).
- ²⁷R. Khasanov, A. Shengelaya, A. Maisuradze, D. Di Castro, I. M. Savić, S. Weyeneth, M. S. Park, D. J. Jang, S.-I. Lee, and H. Keller, *Phys. Rev. B* **77**, 184512 (2008).
- ²⁸J. S. White, E. M. Forgan, M. Laver, P. S. Häfliger, R. Khasanov, R. Cubitt, C. D. Dewhurst, M.-S. Park, D.-J. Jang, H.-G. Lee *et al.*, *J. Phys.: Condens. Matter* **20**, 104237 (2008).
- ²⁹M. L. Teague, A. D. Beyer, M. S. Grinolds, S. I. Lee, and N.-C. Yeh, *Europhys. Lett.* **85**, 17004 (2009).
- ³⁰L. Fruchter, V. Jovanovic, H. Raffy, S. Labdi, F. Bouquet, and Z. Z. Li, *Phys. Rev. B* **82**, 144529 (2010).
- ³¹D. A. Wollman, D. J. Van Harlingen, W. C. Lee, D. M. Ginsberg, and A. J. Leggett, *Phys. Rev. Lett.* **71**, 2134 (1993).
- ³²C. C. Tsuei, J. R. Kirtley, C. C. Chi, L. Yu-Jahnes, A. Gupta, T. Shaw, J. Z. Sun, and M. B. Ketchen, *Phys. Rev. Lett.* **73**, 593 (1994).
- ³³R. R. Schulz, B. Chesca, B. Goetz, C. W. Schneider, A. Schmehl, H. Bielefeldt, H. Hilgenkamp, J. Mannhart, and C. C. Tsuei, *Appl. Phys. Lett.* **76**, 912 (2000).
- ³⁴B. Chesca, R. R. Schulz, B. Goetz, C. W. Schneider, H. Hilgenkamp, and J. Mannhart, *Phys. Rev. Lett.* **88**, 177003 (2002).
- ³⁵J. Tomaschko, V. Leca, T. Selistrovski, R. Kleiner, and D. Koelle, *Phys. Rev. B* **84**, 214507 (2011).
- ³⁶B. Chesca, *Ann. Phys.* **8**, 511 (1999).
- ³⁷J. Tomaschko, C. Raisch, V. Leca, T. Chassé, R. Kleiner, and D. Koelle, *Phys. Rev. B* **84**, 064521 (2011).
- ³⁸J. Tomaschko, V. Leca, T. Selistrovski, S. Diebold, J. Jochum, R. Kleiner, and D. Koelle, *Phys. Rev. B* **85**, 024519 (2012).
- ³⁹See Supplemental Material at <http://link.aps.org/supplemental/10.1103/PhysRevB.86.094509> for additional transport data.
- ⁴⁰M. B. Ketchen, W. J. Gallagher, A. W. Kleinsasser, S. Murphy, and J. R. Clem, *SQUID 85, Superconducting Quantum Interference Devices and Their Applications* (Walter de Gruyter, Berlin, 1985), p. 865.
- ⁴¹R. Straub, S. Keil, R. Kleiner, and D. Koelle, *Appl. Phys. Lett.* **78**, 3645 (2001).
- ⁴²D. Koelle, R. Gross, R. Straub, S. Keil, M. Fischer, M. Peschka, R. P. Huebener, and K. Barthel, *Physica C* **332**, 148 (2000).
- ⁴³A. J. Leggett, *Nat. Phys.* **2**, 134 (2006).
- ⁴⁴D. M. Newns and C. C. Tsuei, *Nat. Phys.* **3**, 184 (2007).
- ⁴⁵R. A. Nistor, G. J. Martyna, D. M. Newns, C. C. Tsuei, and M. H. Müser, *Phys. Rev. B* **83**, 144503 (2011).